

# Surface Phase Separation and Flow in a Simple Model of Multicomponent Drops and Vesicles

J.S. Lowengrub<sup>1</sup>, J.-J. Xu<sup>2</sup> and A. Voigt<sup>3</sup>

(Communicated by Mark Sussman)

**Abstract:** We introduce and investigate numerically a thermodynamically consistent simple model of a drop or vesicle in which the interfacial surface contains multiple constitutive components (e.g. amphiphilic molecules). The model describes the nonlinear coupling among the flow, drop/vesicle morphology and the evolution of the surface phases. We consider a highly simplified version of the Helfrich model for fluid-like vesicle membranes in which we neglect the effects of bending forces and spontaneous curvature but keep the effects of inhomogeneous surface tension forces. Thus, this model may also describe liquid drops. To solve the highly nonlinear, coupled system a new numerical method is developed. This method combines the immersed interface method to solve the flow equations, and the Laplace-Young jump conditions, with the level-set method to represent and evolve the interface and a non-stiff Eulerian algorithm to update the mass concentration on the drop interface. Results are presented for drops/vesicles in an applied shear flow where an initially unstable mixture of the surface mass separates into distinct phases.

## 1 Introduction

In this paper, we introduce and investigate numerically a thermodynamically consistent simple model of a drop or vesicle in which the interfacial surface contains multiple constitutive compo-

nents (e.g. amphiphilic molecules). The model describes the nonlinear coupling among the flow, drop/vesicle morphology and the evolution of the surface phases.

We consider a highly simplified version of the Helfrich model (e.g. see Zhong-can and Helfrich (1989)) for fluid-like vesicle membranes in which we neglect the effects of bending forces and spontaneous curvature but keep the effects of inhomogeneous surface tension forces. Thus, this model may also describe liquid drops. We view this work as preparatory for a more complete study of multicomponent vesicles.

Here, the surface energy of the drop/vesicle is assumed to depend upon the concentration of the surface components (e.g. phase-field). An additional energy is introduced that describes the chemical energy of the surface phases which is taken to be of Cahn-Hilliard type. Together, these result in generalized surface tension forces imparted to the flow. The surface phases evolve according to a high-order, advection-reaction-diffusion equation of Cahn-Hilliard type (e.g. phase-field equation) on the surface. Thermodynamically consistent constitutive relations for the generalized surface tension and the chemical diffusion flux are derived.

Membranes consisting of amphiphilic molecules (i.e. molecules that contain both hydrophilic and hydrophobic groups) are fundamental components of many soft-matter systems (e.g., see Lipowsky and Sackman (1995)). Surfactants and lipid bilayers are common examples. In general, however, biomembranes are very complex structures that play an active and critical role in cell functions and contain lipids, proteins, choles-

---

<sup>1</sup> Department of Mathematics, University of California, Irvine. lowengrb@math.uci.edu. Corresponding author.

<sup>2</sup> Department of Mathematics, University of California, Irvine. jxu@math.uci.edu

<sup>3</sup> Institut für Wissenschaftliches Rechnen, Technische Universität Dresden, Zellescher Weg 12-14, 01062 Dresden, Germany. voigt@caesar.de.

terol, ions, etc. (e.g., see Lipowsky and Sackman (1995); Lipowsky (1991); Alberts, Bray, Lewis, Raff, Roberts, and Watson (1994)). The morphology and structure of membranes play an important role in their biological function (e.g., McMahon and Gallop (2005)). Further, these effects are often coupled. For example, it is increasingly recognized that structural rearrangements in membranes, such as changes in local lipid and/or protein compositions, can lead to the generation of curvature, shape deformation and topological changes that have important biological consequences and locomotion (e.g., Mukherjee and Maxfield (2004); McMahon and Gallop (2005); Lavrenteva, Tsemakh, and Nir (2005)).

There have been many experimental and theoretical studies of lipid bilayer biomembranes and vesicles, which while important in their own right, serve as important models for more complex cell-membranes. Like more complex biomembranes, lipid bilayer biomembranes are flexible, liquid-like and may be inhomogeneous due to the presence several lipid components. Recent experiments of giant unilamellar vesicles (GUVs) have shown that membranes containing ternary mixtures of lipid components and cholesterol may phase separate into binary components (e.g. ordered/disordered liquid phases) leading to coexistence of distinct fluid bilayer domains in the membrane. See, for example, Veatch and Keller (2003); Baumgart, Hess, and Webb (2003); Baumgart, Das, Webb, and Jenkins (2005). Spinodal decomposition, coarsening, viscous fingering, vesicle budding and fission are observed. These phenomena are accompanied by shape changes in the membrane. While there have been many theoretical and numerical studies of homogeneous lipid bilayer biomembranes (e.g. see the reviews Nelson, Piran, and Weinberg (2004); Lipowsky (1991); Lipowsky and Sackman (1995); Pozrikidis (2001, 1992), the recent papers Du, Liu, and Wang (2004, 2006); Campelo and Hernandez-Machado (2006); Biben and Misbah (2003); Biben, Kassner, and Misbah (2005) and the references therein), there are far fewer studies of inhomogeneous systems.

A theory of equilibrium shapes of two-component

vesicles was first developed by Julicher & Lipowsky Julicher and Lipowsky (1996) and was later used successfully Baumgart, Hess, and Webb (2003); Baumgart, Das, Webb, and Jenkins (2005) to compare with experimental results on GUVs. In Taniguchi (1996), a dynamical approach was developed that coupled interface dynamics with a surface phase-field equation. This is analogous to the approach taken here except that in Taniguchi (1996) the effect of flow was not considered. Reduced models (e.g. long-wave type approximations) were considered in Uchida (2002); Ramaswamy, Toner, and Prost (2000); Reigada, Buceta, and Lindenberg (2005b,a) and discrete methods (e.g. Monte-Carlo, dissipative particle dynamics, etc) have been developed to evolve the coupled phase-field/membrane system (e.g. Kumar and Rao (1998); Kumar, Gompper, and Lipowsky (2001); Laradji and Kumar (2004); Ayton, McWhirter, and Voth (2005); Shi and Voth (1993)). The effects of flow were considered only in Ramaswamy, Toner, and Prost (2000) via a reduced model.

Here, we investigate the nonlinear coupling among the flow, drop/vesicle morphology and the evolution of the surface phases using the simplified approach described above. We focus on two-dimensions although our approach extends straightforwardly to three-dimensions. To solve the highly nonlinear, coupled system a new numerical method is developed that builds upon methods we previously developed for interfacial flows with surfactant Xu, Li, Lowengrub, and Zhao (2006). This method combines the immersed interface method to solve the flow equations, and the Laplace-Young jump conditions, with the level-set method to represent and evolve the interface and a non-stiff Eulerian algorithm to update the mass concentration on the drop interface. Results are presented for drops/vesicles in an applied shear flow where an initially unstable mixture of the surface mass separates into distinct phases. As the drop deforms due to the applied shear, phase separation occurs where the surface phase component with smaller surface tension appears at the drop tips where the curvature is largest. When the surface tensions of the phases

are nearly matched, the surface phase is dynamic and the evolution apparently becomes periodic. When the surface tensions of the phases are quite different, on the other hand, the evolution tends toward a steady state with the low surface tension phase occupying the region around the drop tips. The outline of the paper is as follows. In section 2, the governing equations are derived and nondimensionalized. In section 3, the numerical algorithms are described. In section 4, preliminary numerical results are presented. In section 5, conclusions are drawn and future work is discussed.

## 2 Formulation

### 2.1 Governing Equations

Consider a vesicle (or drop) containing one viscous fluid that is surrounded by another viscous (matrix) fluid. Let  $\Sigma$  denote the interface separating the fluids. We assume that the fluids are highly viscous so that the Stokes equations govern the flow:

$$\nabla \cdot \mathbf{T}_i = 0 \quad \text{and} \quad \nabla \cdot \mathbf{u}_i = 0 \quad \text{in} \quad \Omega_i, \quad (1)$$

where  $i = d, m$  denotes the drop and matrix fluid regions respectively,  $\mathbf{T}_i = -p_i \mathbf{I} + \eta_i (\nabla \mathbf{u}_i + \nabla \mathbf{u}_i^T)$  is the stress tensor, and  $p_i$  is the pressure.

Across the interface  $\Sigma$ , the velocity is continuous

$$0 = [\mathbf{u}]_\Sigma \equiv (\mathbf{u}|_{\Sigma, m} - \mathbf{u}|_{\Sigma, d}), \quad (2)$$

and the Laplace-Young jump condition holds

$$[\mathbf{T}\mathbf{n}]_\Sigma = \sigma \kappa \mathbf{n} - \nabla_s \sigma, \quad (3)$$

where  $\sigma$  is the surface tension,  $\mathbf{n}$  is the normal vector to  $\Gamma$  directed towards the matrix fluid,  $\kappa = \nabla \cdot \mathbf{n}$  is the curvature of  $\Gamma$  (positive for spherical/circular interface) and  $\nabla_s$  is the surface gradient. The constitutive law for the surface tension will be derived below (see Eq. (18)). In the far-field, we may apply a flow and so we take the condition

$$\mathbf{u} = \mathbf{u}_\infty \quad \text{on} \quad \partial\Omega, \quad (4)$$

where  $\Omega = \Omega_1 \cup \Omega_2$ . Finally, the interface  $\Sigma(t) = \{\mathbf{x}_\Sigma(t)\}$  moves with the fluid so that

$$\frac{d\mathbf{x}_\Sigma}{dt} = \mathbf{u}. \quad (5)$$

Let us suppose for simplicity that there are at most two surface phases (e.g. lipid components, block-copolymer) and let  $f$  denote the mass concentration of one of the surface phases; the concentration of the other phase is  $\bar{f} - f$ , where  $\bar{f}$  is the total concentration of the surface phases. We assume that no reactions occur and that the phases are confined to the interface. Therefore, the mass of the surface-phase is constant in time:

$$M(t) = \int_{\Sigma(t)} f \, d\Sigma = M(0), \quad (6)$$

where we have implicitly assumed, for simplicity, that the surface density of each phase is equal to one (e.g. we have absorbed the density into  $M$ ). To conserve total mass, we also have  $\int_{\Sigma(t)} \bar{f} \, d\Sigma = \int_{\Sigma(0)} \bar{f} \, d\Sigma$ . Assuming, for simplicity, that  $\bar{f} = F_{\text{tot}}(t)$ , we obtain

$$F_{\text{tot}}(t) = F_{\text{tot}}(0) \frac{|\Sigma(0)|}{|\Sigma(t)|} \quad (7)$$

where  $|\Sigma(t)| = \int_{\Sigma(t)} d\Sigma$  denotes the interfacial length in 2D (or area in 3D). We note that we could have alternatively enforced a local condition on  $\bar{f}$  to account for local interface stretching (this would make  $\bar{f}$  time and space dependent). This is currently under investigation.

Accordingly, the surface concentration  $f$  evolves via a convection-reaction-diffusion equation, which written in Eulerian coordinates, is

$$f_t + \mathbf{u} \cdot \nabla f - \mathbf{n} \cdot \nabla \mathbf{u} \cdot \mathbf{n} f = \nabla_s \cdot \mathbf{J}_s \quad (8)$$

where  $\mathbf{J}_s$  is the surface flux. Below, we will derive the constitutive law for this flux (see Eq. (17)). Note that for incompressible velocities, the term  $-\mathbf{n} \cdot \nabla \mathbf{u} \cdot \mathbf{n}$  describes the local rate of change of the interface area and thus this term in Eq. (8) describes the change in  $f$  due to interface stretching. Note that  $-\mathbf{n} \cdot \nabla \mathbf{u} \cdot \mathbf{n} = \nabla_s \cdot \mathbf{u}_s + \kappa \mathbf{u} \cdot \mathbf{n}$  where  $\mathbf{u}_s$  is the tangential velocity on  $\Sigma$ . See Batchelor (1967); James and Lowengrub (2004); Xu, Li, Lowengrub, and Zhao (2006) for example.

**Constitutive relations.** To complete the formulation, we need to obtain constitutive relations for the surface tension  $\sigma$  and the diffusion flux  $\mathbf{J}_s$ . This is done via an energetic variational approach so that the resulting system is consistent with the second law of thermodynamics and fully couples the surface phase separation with the fluid mechanics. To satisfy the second law of thermodynamics, it is sufficient to obtain a non-increasing free energy functional since this is equivalent to a non-decreasing entropy (e.g., the Helmholtz free energy  $H = e - Ts$  where  $e$  is the internal energy,  $T$  is the temperature and  $s$  is the entropy, e.g. see Landau (1984)). Let us consider the free energy of the system to be

$$E = E_s + E_f, \quad (9)$$

where,

$$E_s = \int_{\Sigma(t)} \gamma(\bar{f}, f) d\Sigma,$$

and

$$E_f = \int_{\Sigma(t)} \left( g(\bar{f}, f) + \frac{\varepsilon^2}{2} |\nabla_s f|^2 \right) d\Sigma,$$

where  $E_s$  is the surface energy and  $E_f$  is a generalized chemical free energy associated with the surface phase which, under appropriate scaling conditions, is the line-energy separating the surface domains. The function  $\gamma(\bar{f}, f)$  is the surface energy density (of the surface phase components),  $g(\bar{f}, f)$  is the chemical free energy (e.g. double-well potential) and  $\varepsilon$  is a parameter (taken to be constant for simplicity) that measures the excess energy due to surface gradients.

Next, we take the time derivative of Eq. (9). This is equivalent to varying both the interface  $\Sigma$  and the function  $f$  simultaneously (and independently). A calculation in Eulerian coordinates shows that

$$\dot{E}_s = \int_{\Sigma(t)} \left( \frac{\partial \gamma}{\partial \bar{f}} \dot{\bar{f}} + \frac{\partial \gamma}{\partial f} \dot{f} - \gamma \mathbf{n} \cdot \nabla \mathbf{u} \cdot \mathbf{n} \right) d\Sigma, \quad (10)$$

where  $\dot{f} = \partial f / \partial t + \mathbf{u} \cdot \nabla f$  and  $\dot{\bar{f}}$  is defined analogously. Note that in defining  $\dot{f}$ , we have implicitly assumed that  $f$  is extended off the interface

such that  $\nabla f \cdot \mathbf{n} = 0$  in a neighborhood of  $\Sigma$ ; thus  $\nabla f = \nabla_s f$  (likewise for  $\dot{\bar{f}}$  if  $\bar{f}$  is space dependent). An similar calculation shows that

$$\begin{aligned} \dot{E}_f = & \int_{\Sigma(t)} \left( \dot{\bar{f}} \frac{\partial g}{\partial \bar{f}} + \dot{f} \left( \frac{\partial g}{\partial f} - \varepsilon^2 \Delta_s f \right) \right. \\ & \left. - \varepsilon^2 \nabla_s f \cdot \nabla \mathbf{u} \cdot \nabla_s f \right) d\Sigma \\ & + \int_{\Sigma(t)} \left( g(f) + \frac{\varepsilon^2}{2} |\nabla_s f|^2 \right) (\mathbf{I} - \mathbf{nn}) : \nabla \mathbf{u} d\Sigma, \end{aligned} \quad (11)$$

where  $\Delta_s = \nabla_s \cdot \nabla_s$  is the Laplace-Beltrami operator (e.g. surface Laplacian) and we have integrated by parts and used the incompressibility of  $\mathbf{u}$ . The notation  $\mathbf{a} : \mathbf{b} = \sum_{ij} a_{ij} b_{ij}$  denotes the tensor product. For simplicity, let us focus on two-dimensions; the 3D problem will be considered in a future work. In 2D,  $\nabla_s f \cdot \nabla \mathbf{u} \cdot \nabla_s f = |\nabla_s f|^2 (\mathbf{I} - \mathbf{nn}) : \nabla \mathbf{u}$ . Putting this together with Eqs. (8), (10) and (11), and assuming that  $\bar{f} = F_{\text{tot}}(t)$  such that

$$\dot{\bar{f}} = - \frac{\bar{f}}{|\Sigma(t)|} \int_{\Sigma(t)} (\mathbf{I} - \mathbf{nn}) : \nabla \mathbf{u} d\Sigma, \quad (12)$$

and integrating by parts we get,

$$\begin{aligned} \dot{E} = & \int_{\Sigma(t)} (\nabla_s \cdot \mathbf{J}_s) \mu d\Sigma \\ & + \int_{\Sigma(t)} \mathbf{u} \cdot (-\nabla_s \xi + \kappa \xi \mathbf{n}) d\Sigma \end{aligned} \quad (13)$$

where  $\mu$  is the chemical potential defined by

$$\mu = \frac{\partial g}{\partial f} - \varepsilon^2 \Delta_s f + \frac{\partial \gamma}{\partial f}, \quad (14)$$

and  $\xi$  is given by

$$\begin{aligned} \xi(f) = & g(\bar{f}, f) - f \frac{\partial g}{\partial f} - \frac{\bar{f}}{|\Sigma(t)|} \int_{\Sigma(t)} \frac{\partial g}{\partial \bar{f}} d\Sigma \\ & - \frac{\varepsilon^2}{2} |\nabla_s f|^2 + \varepsilon^2 f \Delta_s f + \tau(\bar{f}, f) \end{aligned} \quad (15)$$

where  $\tau$  is the surface tension of the surface phase components (i.e. surface tension in the absence of phase separation:  $g = 0$  and  $\varepsilon = 0$ ) given by

$$\tau(\bar{f}, f) = \gamma(\bar{f}, f) - f \frac{\partial \gamma}{\partial f} - \frac{\bar{f}}{|\Sigma(t)|} \int_{\Sigma(t)} \frac{\partial \gamma}{\partial \bar{f}} d\Sigma.$$

(16)

Next, supposing that chemical and viscous dissipation may be separated from one another leads to the constitutive assumption for the flux

$$J_s = v \nabla_s \mu, \quad (17)$$

which is a generalized Fick's law, and the constitutive assumption for the (generalized) surface tension  $\sigma = \xi$ , which therefore yields

$$\begin{aligned} \sigma = g(\bar{f}, f) - f \frac{\partial g}{\partial f} - \frac{\bar{f}}{|\Sigma(t)|} \int_{\Sigma(t)} \frac{\partial g}{\partial \bar{f}} d\Sigma \\ - \frac{\varepsilon^2}{2} |\nabla_s f|^2 + \varepsilon^2 f \Delta_s f + \tau(\bar{f}, f). \end{aligned} \quad (18)$$

Assuming that  $\mathbf{u}_\infty = 0$  and using Eqs. (17), (18) and (3) in Eq. (13) and integrating by parts and using the divergence theorem gives the energy dissipation

$$\begin{aligned} \dot{E} = - \int_{\Sigma(t)} v |\nabla_s \mu|^2 d\Sigma \\ - \frac{1}{2} \int_{\Omega_d} \eta_d (\nabla \mathbf{u}_d + \nabla \mathbf{u}_d^T) : (\nabla \mathbf{u}_d + \nabla \mathbf{u}_d^T) d\mathbf{x} \\ - \frac{1}{2} \int_{\Omega_m} \eta_m (\nabla \mathbf{u}_m + \nabla \mathbf{u}_m^T) : (\nabla \mathbf{u}_m + \nabla \mathbf{u}_m^T) d\mathbf{x}, \end{aligned} \quad (19)$$

Thus, the constitutive assumptions in Eqs. (17) and (18) are consistent with the second law of thermodynamics.

## 2.2 Nondimensionalization

Let the drop radius,  $a$ , be the length scale,  $a/\bar{U}$  be the time scale, where  $\bar{U}$  is a characteristic velocity scale,  $\bar{p} = \eta_m \bar{U}/a$  be the characteristic stress scale and  $\bar{\sigma}$  be a characteristic surface tension scale. Denoting the nondimensional quantities by tildes, i.e.  $\tilde{\mathbf{x}} = \mathbf{x}/a$ ,  $\tilde{\mathbf{T}}_i = \mathbf{T}_i/\bar{p}$ ,  $\tilde{\mathbf{u}}_i = \mathbf{u}_i/\bar{U}$ ,  $\tilde{\sigma} = \sigma/\bar{\sigma}$  etc., we obtain the nondimensional Stokes equations

$$\tilde{\nabla} \cdot \tilde{\mathbf{T}}_i = 0, \quad \tilde{\nabla} \cdot \tilde{\mathbf{u}}_i = 0, \quad \text{where } i = d, m \quad (20)$$

with the stress tensor  $\tilde{\mathbf{T}}_i = -\tilde{p}_i \mathbf{I} + \lambda_i (\tilde{\nabla} \tilde{\mathbf{u}}_i + \tilde{\nabla} \tilde{\mathbf{u}}_i^T)$  and the viscosity ratio  $\lambda_m = 1$  and  $\lambda_d = \eta_d/\eta_m$ . The velocity is continuous across  $\tilde{\Sigma}$  (e.g. Eq. (2) is

satisfied for  $\tilde{\mathbf{u}}_i$ ) and the Laplace-Young condition (3) becomes

$$[\tilde{\mathbf{T}}\tilde{\mathbf{n}}]_{\tilde{\Sigma}} = \frac{1}{Ca} (\tilde{\sigma} \tilde{\kappa} \tilde{\mathbf{n}} - \tilde{\nabla}_s \tilde{\sigma}), \quad (21)$$

where  $Ca = \eta_m \bar{U}/\bar{\sigma}$  is the Capillary number. Letting  $\bar{\mu}$  be the characteristic chemical energy scale, we obtain from Eq. (18), the nondimensional surface tension

$$\begin{aligned} \tilde{\sigma} = \frac{1}{\mathcal{M}} \left( \tilde{g}(\bar{f}, f) - f \frac{\partial \tilde{g}}{\partial f} - \frac{\bar{f}}{|\Sigma(t)|} \int_{\Sigma(t)} \frac{\partial \tilde{g}}{\partial \bar{f}} d\Sigma \right. \\ \left. - \frac{\mathcal{C}^2}{2} |\tilde{\nabla}_s f|^2 + \mathcal{C}^2 f \tilde{\Delta}_s f \right) + \tilde{\tau}(\bar{f}, f) \end{aligned} \quad (22)$$

where  $f$  is already nondimensional,  $\tilde{g} = g/\bar{\mu}$ ,  $\tilde{\tau} = \tau/\bar{\sigma}$ , the Cahn number  $\mathcal{C} = \varepsilon/(a\sqrt{\bar{\mu}})$  and  $\mathcal{M} = \bar{\sigma}/\bar{\mu}$  measures the relative strengths of the surface tension and chemical forces (e.g. this is an analogue of the Mach number, see Lowengrub and Truskinvosky (1998)). Accordingly, the nondimensional chemical potential is given by

$$\tilde{\mu} = \frac{\partial \tilde{g}}{\partial f} - \mathcal{C}^2 \tilde{\Delta}_s f + \mathcal{M} \frac{\partial \tilde{\gamma}}{\partial f}. \quad (23)$$

Further, the nondimensional version of the surface mass transport Eq. (8) is

$$f_t + \tilde{\mathbf{u}} \cdot \tilde{\nabla} f - \tilde{\mathbf{n}} \cdot \tilde{\nabla} \tilde{\mathbf{u}} \cdot \tilde{\mathbf{n}} f = \frac{1}{Pe} \tilde{\nabla}_s \cdot (\tilde{v} \tilde{\nabla}_s \tilde{\mu}) \quad (24)$$

where the Peclet number  $Pe = \bar{v} \bar{\mu}/(a\bar{U})$ . Finally, the nondimensional energy is

$$\begin{aligned} \tilde{E}(\tilde{t}) = \frac{1}{\mathcal{M}} \left( \int_{\tilde{\Sigma}} \tilde{g}(\bar{f}, f) + \frac{\mathcal{C}^2}{2} |\tilde{\nabla}_s f|^2 d\tilde{\Sigma} \right) \\ + \int_{\tilde{\Sigma}} \tilde{\gamma}(\bar{f}, f) d\tilde{\Sigma} \end{aligned} \quad (25)$$

Following Lowengrub and Truskinvosky (1998), the method of matched asymptotic expansions can be applied to show that in the limit  $\mathcal{M} \sim \mathcal{C} \rightarrow 0$  the first term in Eq. (25) converges to the line-energy separating the surface domains. This will be discussed further in a future work. In the remainder of the paper, we drop the tilde notation.

### 3 Numerical methods

We solve the system of equations in 2D using the immersed interface method (IIM) to obtain the fluid flow coupled with the level-set method to capture the interfacial motion. The mass concentration  $f$  is extended to a neighborhood of the interface  $\Sigma$  and a nonstiff algorithm is used to update  $f$ . The algorithm is an extension of the approach we developed in Xu, Li, Lowengrub, and Zhao (2006) for interfacial flows with surfactants. For simplicity, we consider the case of viscosity matched fluids  $\lambda = 1$ . We note that our algorithm extends straightforwardly to 3D. The IIM can also be extended to the case in which the viscosity ratio  $\lambda \neq 1$  by using an augmented variable approach Li, Ito, and Lai (2007).

#### 3.1 The IIM for the Stokes equations

The IIM is a second order accurate method using a Cartesian mesh that incorporates the jump conditions directly into the difference stencil (e.g., see LeVeque and Li (1994, 1997)). The IIM is based on decomposing the Stokes equations (20)-(21) into three Poisson equations— one for the pressure and two for the velocity (i.e. one equation for each velocity component). At time  $t_k$ , the equation for the pressure  $p^k = p(\mathbf{x}, t_k)$  is obtained by taking the divergence of Eq. (20). Assuming  $\lambda = 1$ , this gives

$$\nabla^2 p^k = 0 \quad (26)$$

with jump boundary conditions on  $\Sigma^k$ :

$$[p^k]_{\Sigma^k} = - \left( \frac{1}{Ca} \sigma \kappa \right)^k, \quad \left[ \frac{\partial p}{\partial n} \right]_{\Sigma^k} = \left( \frac{1}{Ca} \nabla_s^2 \sigma \right)^k, \quad (27)$$

and Neumann boundary conditions on  $\partial\Omega$ :

$$\left( \frac{\partial p}{\partial n} \right)^k = \begin{cases} 2(\nabla^2 \mathbf{u} \cdot \mathbf{n})^{k-1} - (\nabla^2 \mathbf{u} \cdot \mathbf{n})^{k-2}, & k \geq 2 \\ (\nabla^2 \mathbf{u} \cdot \mathbf{n})^{k-1}, & k = 1 \end{cases} \quad (28)$$

Once the pressure is determined, the velocity  $\mathbf{u}^k$  is obtained by solving the Poisson system (again assuming  $\lambda = 1$ ):

$$\nabla^2 \mathbf{u}^k = \nabla p^k, \quad (29)$$

together with the jump boundary conditions on  $\Sigma^k$  LeVeque and Li (1997):

$$[\mathbf{u}^k]_{\Sigma^k} = 0, \quad \left[ \frac{\partial \mathbf{u}^k}{\partial n} \right]_{\Sigma^k} = \left( \frac{1}{Ca} \nabla_s \sigma \right)^k. \quad (30)$$

and the far-field Dirichlet boundary condition

$$\mathbf{u}^k = \mathbf{u}_\infty^k \quad \text{on } \partial\Omega. \quad (31)$$

The interface  $\Sigma^k$  is represented by the zero set of the level-set function  $\phi^k = \phi(\mathbf{x}, t_k)$ , i.e.  $\Sigma^k = \{\mathbf{x} : \phi(\mathbf{x}, t_k) = 0\}$ . Assume that  $\{\mathbf{x} : \phi(\mathbf{x}, t) < 0\} = \Omega_d$ , then the outward normal and curvature are

$$\mathbf{n}^k = \frac{\nabla \phi^k}{|\nabla \phi^k|}, \quad \kappa^k = \nabla \cdot \left( \frac{\nabla \phi^k}{|\nabla \phi^k|} \right) \quad (32)$$

The evolution of  $\phi$  is described below in section 3.2.

The Poisson equations for the pressure and velocity are discretized as follows. First, the grid points are divided into two groups. All grid points that are adjacent to the interface classified as irregular grid points, while the remaining points are termed regular. The interface position is approximated by the intersections of the zero level-set of  $\phi$  and the grid lines, assuming  $\phi$  is locally piecewise linear.

At the regular grid points, a standard centered difference scheme is used to discretize the Poisson equations. At the irregular grid points, the standard center difference scheme is modified by adding a correction term to account for the jumps. The correction term, which modifies only the right hand side of the equation, can be derived from the two jump conditions, a Taylor series expansion of the solution in local coordinates and the method of undetermined coefficients to yield a second order accurate discretization (see LeVeque and Li (1994); Xu, Li, Lowengrub, and Zhao (2006)). Note that an alternative approach, the ghost fluid method (GFM, e.g. see Fedkiw, Aslam, Merriman, and Osher (1999); Kang, Fedkiw, and Liu (2000); Gibou and Fedkiw (2005); Macklin and Lowengrub (2005, 2006)), can be used. However, in the GFM, no expansions are performed and the coordinate directions are used to perform one-sided extrapolations. The GFM

can be problematic when there is a jump in the solution because tangential jumps are smeared out, thus reducing the order of accuracy. This does not occur using in the IIM. In order to approximate the jump conditions at the interface, the surface tension (and mass concentration) and its derivatives, are computed at grid points in a local tube around the interface (see below) and are interpolated to the approximate interface position.

The resulting scheme has local truncation error  $O(h^2)$  at regular grid points (where  $h$  is the spatial grid size), and  $O(h)$  at irregular grid points. Since the whole set of irregular grid points is of co-dimension one, global second order accuracy can be achieved LeVeque and Li (1997, 1994). The resulting discrete systems are solved by using the FFT.

### 3.2 Interface capturing using the level-set function

The level-set method, first introduced by Osher and Sethian (1988), has been highly successful in describing interface dynamics in many applications including multiphase flows. See the recent reviews Osher and Fedkiw (2001); Sethian and Smereka (2003), for example. Here, we follow our previous work Xu, Li, Lowengrub, and Zhao (2006) and use the level-set method to capture the interface motion. Since the interface moves with the fluid, we take

$$\frac{\partial \phi}{\partial t} + \mathbf{u} \cdot \nabla \phi = 0, \quad (33)$$

although  $\mathbf{u}$  need not correspond to the fluid velocity away from the interface (e.g. Adalsteinsson and Sethian (1999); Macklin and Lowengrub (2005)).

The level-set function is re-initialized after each time step to be a signed distance function locally near the interface Sussman, Smereka, and Osher (1994). This is performed by solving the following Hamilton-Jacobian equation to steady state

$$\begin{cases} \phi_\tau + S(\phi_0)(|\nabla \phi| - 1) = 0 \\ \phi(\mathbf{x}, 0) = \phi_0(\mathbf{x}) \end{cases} \quad (34)$$

where  $\phi_0$  is the level set function before the re-initialization,  $\tau$  is the pseudo-time and  $S(x)$  is the

sign function of  $x$  defined as

$$S(x) = \begin{cases} -1 & \text{if } x < 0, \\ 0 & \text{if } x = 0, \\ 1 & \text{if } x > 0. \end{cases} \quad (35)$$

In practice, the re-initialization is performed at every time step.

In the above equations, the standard third order upwinding WENO method Jiang and Peng (2000) is used for the spatial discretization and the standard third order TVD Runge-Kutta method Shu (1988) is used for time time stepping. A smoothed approximation of the sign function (35) is used,

$$\tilde{S}(\phi) = \frac{\phi}{\sqrt{\phi^2 + h^2}}, \quad (36)$$

where as before  $h$  is the spatial grid size.

### 3.3 The evolution of the mass concentration

The mass concentration  $f$  is evolved in two steps. First,  $f$  and the chemical potential  $\mu$  are extended off the interface  $\Sigma$  into a small tube around  $\Sigma$ . Second, the surface mass transport Eq. (24) is solved in the tube using an efficient non-stiff method.

#### 3.3.1 Extension of the mass concentration off the interface

Using the level set methodology,  $f$  is extended off  $\Sigma$  by solving the following Hamilton-Jacobian equation Zhao, Chan, Merriman, and Osher (1996):

$$\begin{cases} f_\tau + S(\phi) \mathbf{n} \cdot \nabla f = 0, \\ f(\mathbf{x}, 0) = f_0(\mathbf{x}) \end{cases} \quad (37)$$

where as before  $S(x)$  is the sign function of  $x$  defined in Eq. (35) and  $\tau$  is a pseudo-time. The pseudo-time  $\tau$  measures the magnitude of the radius of the tube into which  $f$  is extended. The chemical potential  $\mu$  is extended off  $\Sigma$  analogously. Eq. (37) is solved using the third order WENO and Runge-Kutta spatial and temporal discretizations, respectively.

### 3.3.2 A nonstiff method for the surface mass transport equation

The surface mass transport equation (24) is a non-linear, fourth-order equation involving advection, interface stretching and surface chemical diffusion. Explicit time integration methods, therefore, require severe (4th order) restrictions upon the time step for stability. To overcome this difficulty, we develop a new, non-stiff semi-implicit numerical method in which the highest order terms are integrated implicitly in time.

For simplicity, we assume that the mobility  $\nu = 1$ . Then, following Xu and Zhao (2003), we decompose the Laplace-Beltrami operator as

$$\Delta_s \mu = \Delta \mu - \frac{\partial^2 \mu}{\partial n^2} - \kappa \frac{\partial \mu}{\partial n}, \quad (38)$$

where  $\Delta = \partial^2 / \partial x^2 + \partial^2 / \partial y^2$  is the usual Laplacian, and following Eyre (1998) we decompose the Helmholtz free energy

$$\frac{\partial g}{\partial f} = \bar{a}f + \left( \frac{\partial g}{\partial f} - \bar{a}f \right), \quad (39)$$

where  $\bar{a}$  is a nonnegative constant ( $\bar{a}$  is typically taken to be  $\max \left| \frac{\partial^2 g}{\partial f^2} \right|$ ). We then rewrite Eq. (24) as the vector system:

$$f_t - \frac{1}{Pe} \Delta \mu = F(\mathbf{x}, t), \quad (40)$$

$$\mu - \bar{a}f + \mathcal{C}^2 \Delta f = G(\mathbf{x}, t), \quad (41)$$

where

$$F(\mathbf{x}, t) = -\mathbf{u} \cdot \nabla f + \mathbf{n} \cdot \nabla \mathbf{u} \cdot \mathbf{n} f - \frac{1}{Pe} \left( \frac{\partial^2 \mu}{\partial n^2} + \kappa \frac{\partial \mu}{\partial n} \right), \quad (42)$$

$$G(\mathbf{x}, t) = \frac{\partial g}{\partial f} - \bar{a}f + \frac{\partial \gamma}{\partial f} + \mathcal{C}^2 \left( \frac{\partial^2 f}{\partial n^2} + \kappa \frac{\partial f}{\partial n} \right), \quad (43)$$

and except for the advection term  $\mathbf{u} \cdot \nabla f$ , we use centered differences in space and a semi-implicit backward Euler discretization in time to discretize

the system (40)-(41). The advection term is discretized using third order WENO. The left hand sides of Eqs. (40)-(41) are discretized implicitly while the right hand sides are discretized explicitly. The resulting linear system is solved in a band around the interface by using a block Gauss-Seidel method for  $f$  and  $\mu$  simultaneously. Using an error tolerance of  $10^{-6}$ , less than 50 iterations per time step are required. Because the number of updated points scales like  $N$ , where  $N$  is the number of grid points in a one direction, this algorithm is still inexpensive. However, other more efficient solution methods (e.g. multigrid) are under development.

### 3.4 Enforcing area and surface mass conservation

One of the drawbacks of the level-set method is that area (volume) of the drop is not exactly conserved by the flow. In addition, the mass of  $f$  is not exactly conserved by our algorithm either. Typically, small errors in each step of the algorithm are incurred at every time step and after long times these errors may accumulate and lead to inaccurate results. Interestingly, we find that the most significant source of mass error arises from the fact that the discrete velocity field obtained from the IIM is not exactly divergence free Xu, Li, Lowengrub, and Zhao (2006). Therefore, to enforce area conservation, a small correction is added to the normal velocity of each moving interface. This is an approach frequently used in boundary integral simulations (e.g. see Cristini, Blawdziewicz, and Loewenberg (2001)). Let  $\tilde{\mathbf{u}}_h$  be the discrete velocity obtained from the IIM. we determine a small correction  $\alpha$  to ensure that the net mass flux across the interface is zero.

$$\int_{\Sigma} (\tilde{\mathbf{u}}_h + \alpha \mathbf{n}) \cdot \mathbf{n} ds = 0.$$

This yields the explicit expression

$$\alpha = -\frac{\int_{\Sigma} \tilde{\mathbf{u}}_h \cdot \mathbf{n} ds}{\int_{\Sigma} ds} = -\frac{\int \tilde{\mathbf{u}}_h \cdot \mathbf{n} \delta_{\Sigma}(\phi) d\mathbf{x}}{\int \delta_{\Sigma}(\phi) d\mathbf{x}}, \quad (44)$$

The modified velocity is then used to advect the level set function and the surface mass concentration  $f$ . The modification above ensures that the

total mass flux across the interface is zero and is found to result in dramatically reduced mass loss overall Xu, Li, Lowengrub, and Zhao (2006).

The above modified velocity also improves the conservation of  $f$ , however there is still significant loss of total surface mass long-times due to numerical diffusion. The simplest way to enforce this correction is to multiply the mass concentration  $f$  by a constant factor to ensure that total surface mass is conserved. Let  $\tilde{f}_h$  be the solution of the discrete surface mass concentration equation and let  $f_0$ ,  $\phi_0$  and  $\Sigma_0$  be the initial mass concentration, level-set function and interface respectively. Then, we choose  $\beta$  such that

$$\int_{\Sigma} \beta \tilde{f}_h d\Sigma = \int_{\Sigma_0} f_0 d\Sigma_0, \quad (45)$$

which yields

$$\beta = \frac{\int_{\Sigma_0} f_0 d\Sigma_0}{\int_{\Sigma} \tilde{f}_h d\Sigma} = \frac{\int_{\Omega} f_0 \delta_{\Sigma_0} d\mathbf{x}}{\int_{\Omega} \tilde{f}_h \delta_{\Sigma} d\mathbf{x}} \quad (46)$$

The mass concentration is then reset to be  $f_h = \beta \tilde{f}_h$ . We refer the reader to Xu and Zhao (2003) for numerical approximations of the delta function in the above integrals noting that  $\delta_{\Sigma} = \delta(\phi)|\nabla\phi|$ .

Finally, we note that other, more sophisticated area and surface mass concentration corrections can be derived that take into account the interface curvature and mass concentration gradients, etc. Nevertheless, we found it sufficient to use the simpler corrections described above.

#### 4 Numerical results

We next perform numerical simulations of surface phase separation coupled to drop dynamics under an applied shear flow  $\mathbf{u}_{\infty} = y\mathbf{e}_y$ . For simplicity, we suppose that the surface energy and chemical energy are independent of  $\bar{f}$ . This is most appropriate, for example, when drop deformations are small such that  $\bar{f}$  has small variation. The effect of variable  $\bar{f}$  is under investigation. Assuming  $\bar{f} \approx 1$  (i.e.,  $F_{\text{tot}}(0) = 1$  and  $|\Sigma(0)| \approx |\Sigma(t)|$ ), we take the chemical free energy to be  $g(\bar{f}, f) = f^2(1-f)^2/4$  which is double-welled. That is, the states  $f = 0$  and  $f = 1$  are energetically preferred by the chemical energy.

The surface tension of the components is taken to be  $\tau(\bar{f}, f) = 1 - xf$ , where  $x$  measures the reduction in surface tension by the phase  $f = 1$ . From the nondimensional form of Eq. (16) it follows that the surface energy is  $\gamma(\bar{f}, f) = 1 + xf \log f$ . In practice, the logarithmic contribution to the chemical potential  $\mu$ , given by  $\gamma'$ , is mollified as  $\log f \approx 1/2 \log(f^2 + \mathcal{C}^2)$ .

The initial interface is a circle of radius 0.5 located at the origin. The computational domain is  $\Omega = [-1, 1] \times [-1, 1]$ . The initial concentration field on  $\Sigma$  is a small, nonsymmetric perturbation of the unstable state 0.5. In particular, we take  $f(x, y, 0) = 0.5 + 0.01(\sin x \cos y + \sin(4x) \cos(3y))$ . See Figs. 1[a] and 2[a]. In the simulations presented below, the grid size is  $h = 0.01$  and the time step is  $\Delta t = h$ . We further note that in the simulations below (up to time 200), the relative errors of drop area and mass of the surface phase are both on the order of 0.2% while the area and mass correction factors are  $|\alpha| \sim 10^{-2}$  and  $|\beta - 1| \sim 10^{-4}$ .

We take the Capillary number  $Ca = 0.2$ , the Peclet number  $Pe = 10$ , the Cahn number  $\mathcal{C} = 0.02$ , and the Mach number  $\mathcal{M} = 1$ . The parameter  $\bar{a} = 0.25$ . We consider two cases:  $x = 0.1$  and  $x = 0.5$ . In the former case, the surface tension  $\tau$  of the components is nearly matched while in the latter case, the surface tension of the components differs significantly. We then determine the effect of the surface tension differences and the flow on the surface phase separation and drop/vesicle morphology.

In Fig. 1, the morphologies are shown, for the case with  $x = 0.1$ , together with the mass concentration  $f$  along the interface. The color scale ranges from 0 (blue) to 1 (red). The morphologies are shown at the times indicated in the caption. At early times, the interface deforms due to the applied shear flow and the surface phase is swept towards the drop tips. Phase separation then rapidly occurs yielding two large regions of  $f \approx 1$  at the drop tips where the curvature is largest. Note that the surface tension of component  $f = 1$  is smaller than that for the  $f = 0$  phase (i.e.  $\tau(1) = 0.9 < \tau(0) = 1.0$ ) so that this part of the generalized surface tension  $\sigma$  favors having

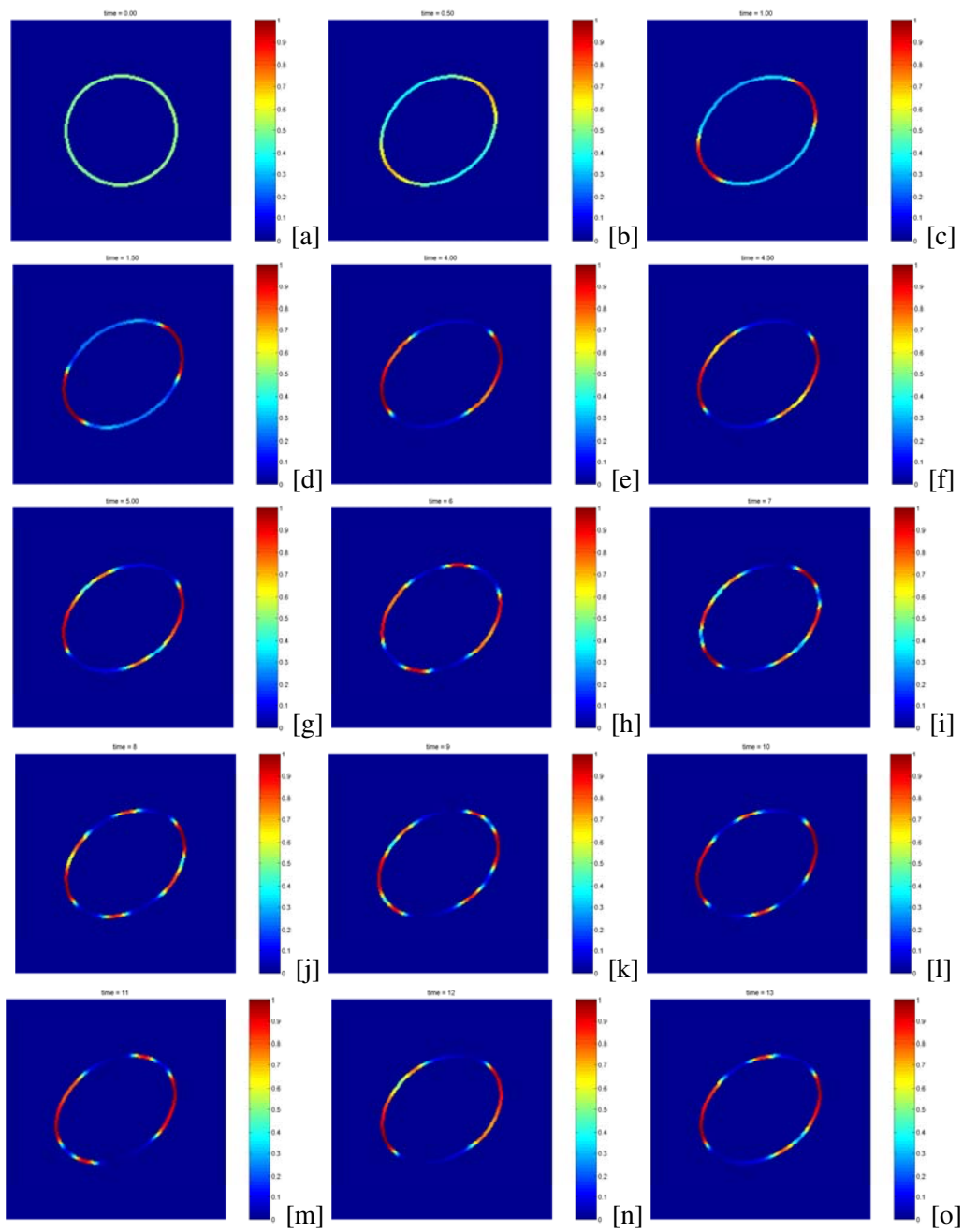


Figure 1: Distribution of mass concentration  $f$  along the interface for  $x = 0.10$ ,  $Ca = 0.2$ ,  $Pe = 10$ ,  $\mathcal{C} = 0.02$ , and  $\mathcal{M} = 1.0$  at times  $t=0$  [a],  $0.5$  [b],  $1.0$  [c],  $1.5$  [d],  $4.0$  [e],  $4.5$  [f],  $5.0$  [g],  $6.0$  [h],  $7.0$  [i],  $8.0$  [j],  $9.0$  [k],  $10.0$  [l],  $11.0$  [m],  $12.0$  [n],  $13.0$  [o].

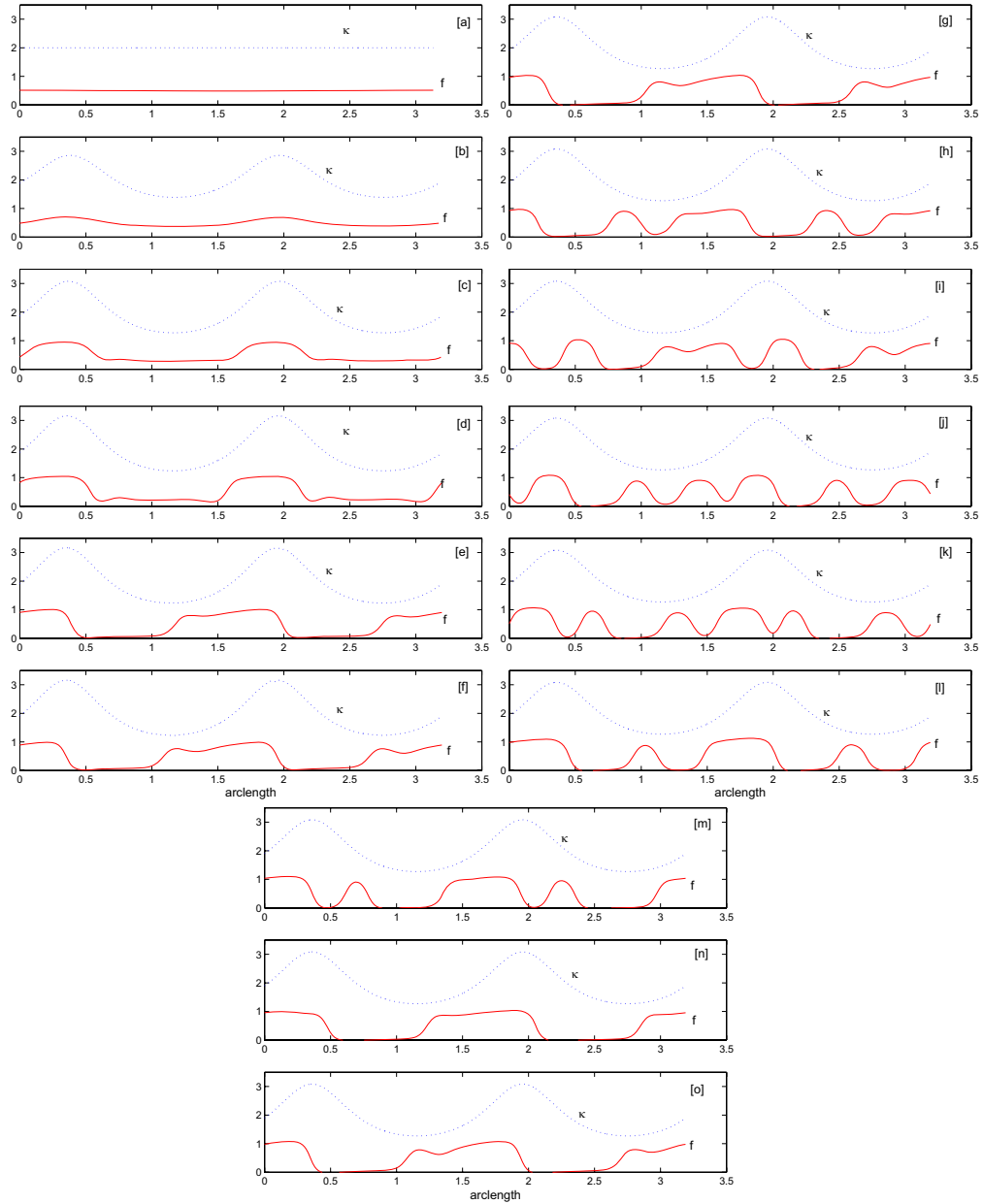


Figure 2: Distribution of mass concentration  $f$  (solid) and curvature  $\kappa$  (dotted) as a function of arclength for the simulation in Fig. 1. Labels and times as in that figure.

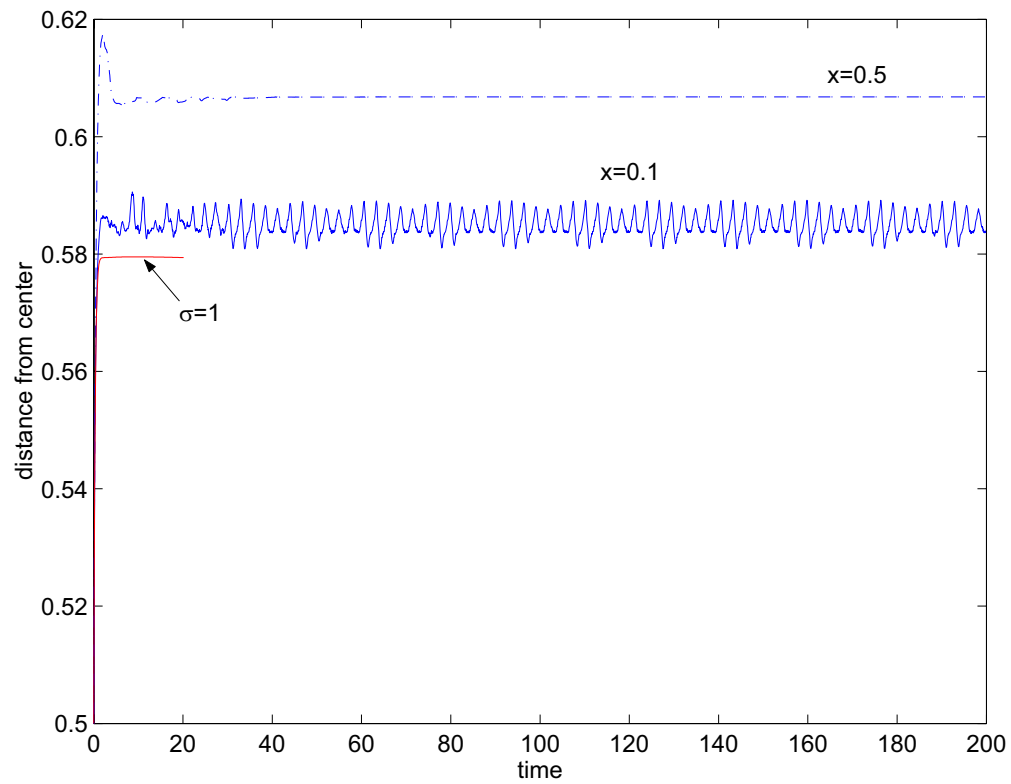


Figure 3: Maximum distance from the center of the drop to the interface as a function of time. Dot-dashed ( $x = 0.5$ ), solid ( $x = 0.1$ ). The other parameters are  $Ca = 0.2$ ,  $Pe = 10$ ,  $\mathcal{C} = 0.02$ , and  $\mathcal{M} = 1.0$ . The curve indicated by  $\sigma = 1$  corresponds to a drop with  $f = 0$  (i.e. single-phase).

the  $f = 1$  phase located in the regions of large curvature at the drop tips. An analysis (not shown) in fact indicates that the difference  $|\sigma - \tau| \approx 10^{-2}$  so that  $\tau$  dominates  $\sigma$ .

Due to the nonlinear coupling between the shape, flow and phase separation, the large  $f \approx 1$  regions that form initially at the drop tips do not remain there. Instead, these large regions move slightly, lengthen and eventually break-off small  $f \approx 1$  regions that travel around the interface. These small regions merge with the large regions on the opposite side of the drop and the process repeats. This can be seen also in Fig. 2 where the mass concentration  $f$  (solid) and interface curvature  $\kappa$  (dotted) are plotted as a function of arclength  $s$  at the same times as shown in Fig. 1. Here  $s = 0$  corresponds to the point on the interface  $\mathbf{x}_\Sigma(0)$  for which the vector  $(\mathbf{x}_\Sigma(0) - \mathbf{x}_{center}) \cdot \mathbf{e}_y = 0$ , where  $\mathbf{x}_{center}$  is the position of the drop center ( $\mathbf{x}_{center} = 0$ ). The arclength is taken to increase in the counterclockwise direction around the drop. Note that at some times and locations  $f$  slightly exceeds one while in other locations  $f$  may also become slightly negative. This is due to the finiteness of  $\mathcal{C}$  and the polynomial form of the chemical energy  $g$  which does not require the mass concentration to lie between zero and one. Other free energies, e.g. the regular solution model free energy, would impose such a restriction (e.g. see Elliot and Luckhaus (1991)). We note that these small deviations outside the interval  $[0, 1]$  are typical of phase-field models with polynomial free energies and do not affect the results.

The process of repeatedly similar break-up and reconnection of large and small  $f \approx 1$  regions on the drop interface seen in Figs. 1 and 2 is suggestive of periodic evolution. To investigate this further, we plot in Fig. 3 the maximum distance  $d(t) = \max |\mathbf{x}_\Sigma - \mathbf{x}_{center}|$  as a function of time  $t$ . Note that  $d(0) = 0.5$ . After an initial transient whereby  $d$  increases rapidly due to the deformation induced by the applied shear flow, the distance  $d$  stabilizes and becomes oscillatory about the value  $d \approx 0.585$ . This indicates that the drop is actually oscillating very slightly due to nonlinear coupling between the flow, shape and phase separation. An analysis of the data suggests that the

motion at later times is very nearly periodic with a period  $16 < T_{period} < 17$ . The development of a potentially periodic evolution under these conditions is quite intriguing and is currently under study.

We next contrast the oscillatory/periodic behavior when  $x = 0.1$  to a case when the surface tension  $\sigma$  is constant. In this case, there is no coupling between the mass concentration and the flow field. The corresponding maximum distance  $d(t)$  is plotted in Fig. 3 as the curve marked  $\sigma = 1$ . After an initial transient,  $d(t)$  settles down to a value  $d \approx 0.58$  and no oscillations are observed, in contrast to the  $x = 0.1$  case. Note that the maximum distance  $d$  for the case with  $x = 0.1$  is larger than that for the case with  $\sigma = 1$ . This is consistent with the surface tension decrease associated with the  $f = 1$  phase.

We lastly turn to the case with  $x = 0.5$ . In Fig. 4, the drop morphologies are shown together with  $f$  along the interface. The morphologies are shown at the times indicated in the caption. In Fig. 5, the corresponding  $f$  (solid) and  $\kappa$  (dotted) are plotted as functions of arclength. At early times, the behavior is qualitatively very similar to that observed when  $x = 0.1$ . The interface deforms and phase separation rapidly occurs leading to large regions of  $f \approx 1$  located at the drop tips. Unlike the  $x = 0.1$  case, however, when  $x = 0.5$  the large  $f \approx 1$  regions remain localized at the drop tips. This is likely because the large surface tension difference between the  $f = 0$  and  $f = 1$  phases makes it much more favorable for the  $f = 1$  phase to be located at the drop tip where the largest interface curvature is achieved. This then leads to the development of a steady-state. This is confirmed by Fig. 3 in which the maximum distance  $d(t)$  is plotted. Observe that during the initial transient, the drop overshoots its steady state shape as  $d$  has a global maximum at this early time. As time increases, small oscillations of decreasing amplitude are seen as  $d$  tends toward the steady value  $d \approx 0.605$ . In this case, the drop is more deformed than either the  $x = 0.1$  and the  $\sigma = 1$  cases which is consistent with the fact that when  $x = 0.5$ , the surface tension of the  $f = 1$  phase ( $\tau(1) = 0.5$ ) is much smaller than that when

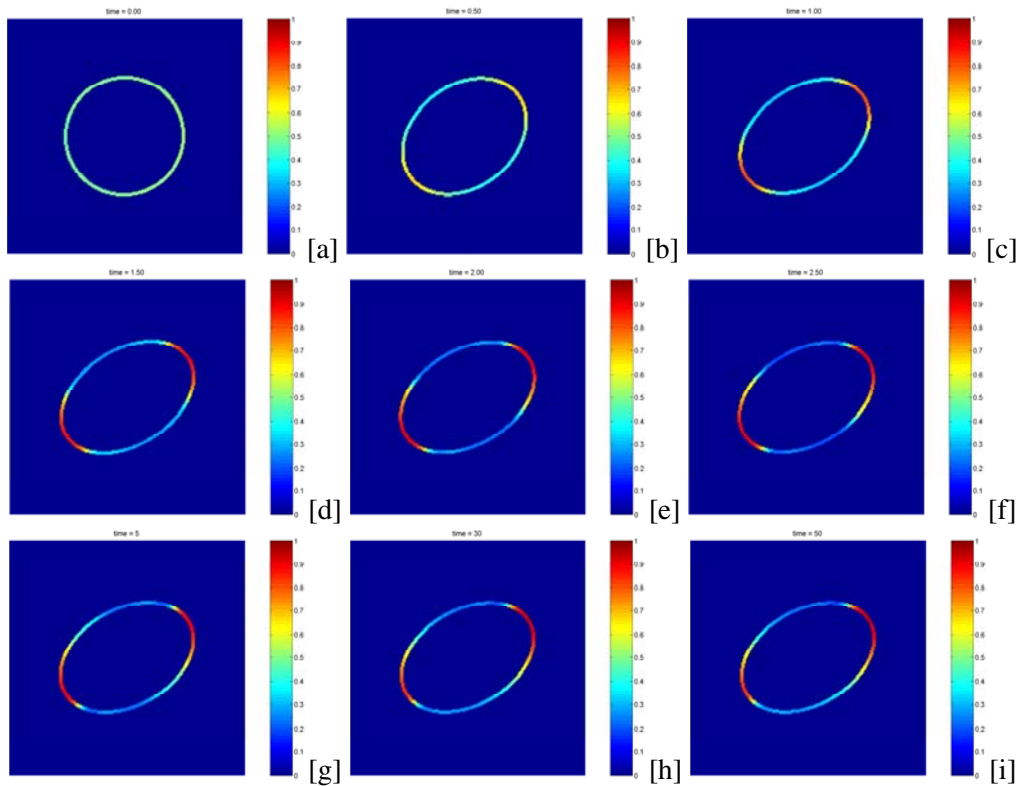


Figure 4: Distribution of mass concentration  $f$  along the interface for  $x = 0.50$ ,  $Ca = 0.2$ ,  $Pe = 10$ ,  $\mathcal{C} = 0.02$ , and  $\mathcal{M} = 1.0$ , at times  $t=0$  [a],  $0.5$  [b],  $1.0$  [c],  $1.5$  [d],  $2.0$  [e],  $2.5$  [f],  $5.0$  [g],  $30.0$  [h],  $50.0$  [i].

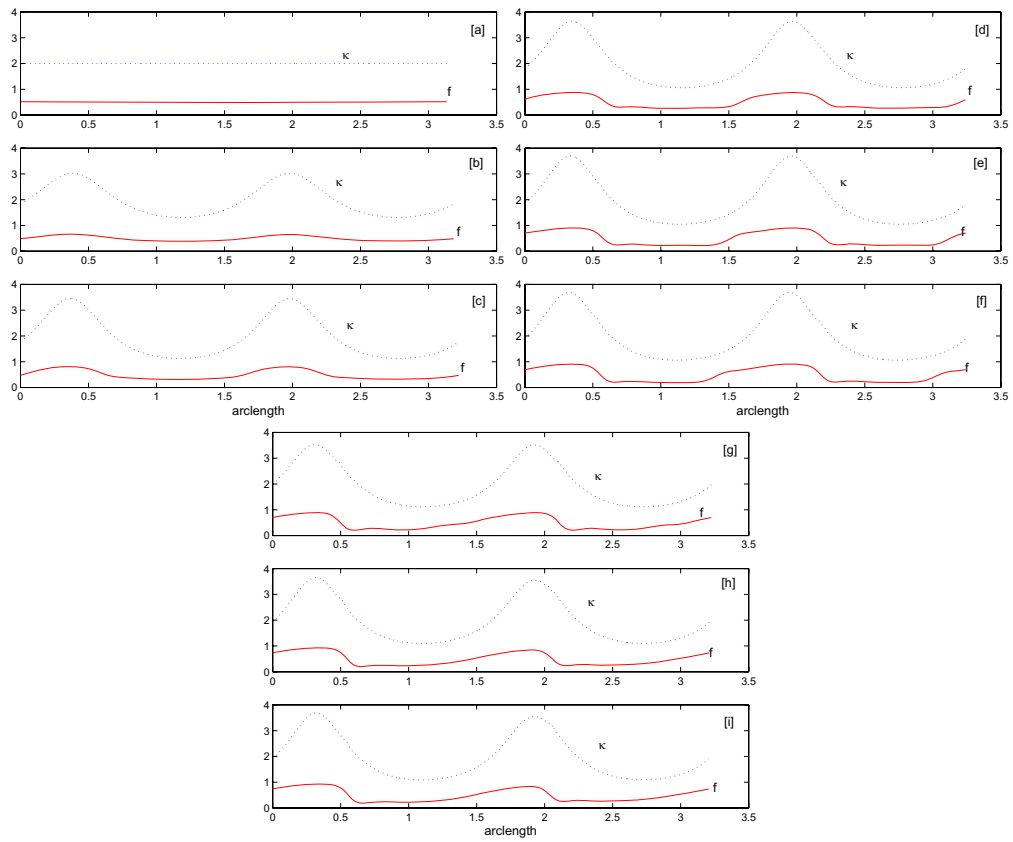


Figure 5: Distribution of mass concentration  $f$  (solid) and curvature  $\kappa$  (dotted) as a function of arclength for the simulation in Fig. 4. Labels and times as in that figure.

$x = 0.1$  and when  $\sigma = 1$ .

## 5 Conclusions and future work

We have introduced and investigated a simple model of a drop or vesicle in which the drop surface contains multiple constitutive components. The model nonlinearly couples fluid flow with the drop morphology and the evolution of the surface phases. The coupling between the morphology and surface phases on the flow occurred through a generalized surface tension. The surface phases evolve according to a high-order, advection, reaction-diffusion equation of Cahn-Hilliard type on the surface. Constitutive relations for the generalized surface tension and the diffusion flux are proposed, based on an energetic variational approach, that guarantees that the free energy of the system is nonincreasing (e.g. entropy is non-decreasing).

To solve the highly nonlinear, coupled system a new numerical method is developed that is based upon methods we previously developed for interfacial flows with surfactant Xu, Li, Lowengrub, and Zhao (2006). This method combines the immersed interface method to solve the flow equations, and the Laplace-Young jump conditions, with the level-set method to represent and evolve the interface and a non-stiff Eulerian algorithm to update the mass concentration on the drop interface. Results were presented for drops/vesicles in an applied shear flow where an initially unstable mixture of the surface mass separated into distinct phases. As the drop deforms due to the applied shear, phase separation occurs where the low surface tension, surface phase component appears at the drop tips where the curvature is largest. When the surface tension of the phases is nearly matched, the surface phase is dynamic and the evolution apparently becomes periodic. When the surface tension of the phases is quite different, on the other hand, the evolution tends toward a steady state with the low surface tension phase occupying the region around the drop tips. Thus, the surface tension difference between the phases is a key variable in determining the subsequent dynamics and steady-state configuration.

In the future, we plan to make the model more realistic by including the effects of a time and space dependent total concentration  $\bar{f}$  as well as all the effects described in the Helfrich model of vesicles (e.g. see Zhong-can and Helfrich (1989)) including bending forces and spontaneous curvature. In addition, we plan to explore the effects of inextensibility on the evolution by introducing local tensile forces on the vesicle surface to constrain the interface length locally. We will also extend our algorithms to three-dimensions.

**Acknowledgement:** The authors thank Vittorio Cristini, Shuwang Li and Steven Wise for illuminating and enjoyable discussions. The authors also thank the reviewers for insightful comments. The authors are also grateful for partial support from the National Science Foundation, Division of Mathematical Sciences.

## References

- Adalsteinsson, D.; Sethian, J.** (1999): The fast construction of extension velocities in level set methods. *J. Comp. Phys.*, vol. 148, pp. 2–22.
- Alberts, B.; Bray, D.; Lewis, J.; Raff, M.; Roberts, K.; Watson, J.** (1994): *Molecular biology of the cell*. Garland, New York.
- Ayton, G.; McWhirter, J.; Voth, G.** (2005): Coupling field theory with continuum mechanics: A simulation of domain formation in giant unilamellar vesicles. *Biophys. J.*, vol. 88, pp. 3855.
- Bachelor, G.** (1967): *An introduction to fluid mechanics*. Cambridge University Press, New York.
- Baumgart, T.; Das, S.; Webb, W.; Jenkins, J.** (2005): Membrane elasticity in giant vesicles with fluid phase coexistence. *Biophys. J.*, vol. 89, pp. 1067.
- Baumgart, T.; Hess, S.; Webb, W.** (2003): Imaging coexisting fluid domains in biomembrane models coupling curvature and line tension. *Nature*, vol. 425, pp. 821.

- Biben, T.; Kassner, K.; Misbah, C.** (2005): Phase-field approach to three-dimensional vesicle dynamics. *Phys. Rev. E*, vol. 72, pp. 049121.
- Biben, T.; Misbah, C.** (2003): Tumbling of vesicles under shear flow within an advected-field approach. *Phys. Rev. E*, vol. 67, pp. 031908.
- Campelo, F.; Hernandez-Machado, A.** (2006): Dynamic model and stationary shapes of fluid vesicles. *Eur. Phys. J. E*, vol. 20, pp. 37.
- Cristini, V.; Blawdziewicz, J.; Loewenberg, M.** (2001): An adaptive mesh algorithm for evolving surfaces: Simulations of drop breakup and coalescence. *J. Comp. Phys.*, vol. 168, pp. 445–463.
- Du, Q.; Liu, C.; Wang, X.** (2004): A phase-field approach in the numerical study of the elastic bending energy for vesicle membranes. *J. Comp. Phys.*, vol. 198, pp. 450.
- Du, Q.; Liu, C.; Wang, X.** (2006): Simulating the deformation of vesicle membranes under elastic bending energy in three dimensions. *J. Comp. Phys.*, vol. 212, pp. 757.
- Elliot, C.; Luckhaus, S.** (1991): A generalized diffusion equation for phase separation of a multi-component mixture with interfacial free energy. Inst. for Math. and Appl., Report number 887, 1991.
- Eyre, D.** (1998): Unconditionally gradient stable time marching in the cahn-hilliard equation. In *Computational and mathematical models of microstructural evolution – Mater. Res. Soc. Sympos. Proc.*, volume 529, pp. 39–46. MRS.
- Fedkiw, R.; Aslam, T.; Merriman, B.; Osher, S.** (1999): A nonoscillatory eulerian approach to interfaces in multimaterials flows (the ghost fluid method). *J. Comp. Phys.*, vol. 152, pp. 457–492.
- Gibou, F.; Fedkiw, R.** (2005): A fourth order accurate discretization for the laplace and heat equations on arbitrary domains with applications to the stefan problem. *J. Comp. Phys.*, vol. 202, pp. 577.
- James, A.; Lowengrub, J.** (2004): A surfactant-conserving volume-of-fluid method for interfacial flows with insoluble surfactant. *J. Comput. Phys.*, vol. 201, pp. 685–722.
- Jiang, G.-S.; Peng, D.** (2000): Weighted eno schemes for hamilton-jacobi equations. *SIAM J. Sci. Comput.*, vol. 21, pp. 2126.
- Julicher, F.; Lipowsky, R.** (1996): Shape transformations of vesicles with intramembrane domains. *Phys. Rev. E*, vol. 53, pp. 2670.
- Kang, M.; Fedkiw, R.; Liu, X.** (2000): A boundary condition capturing method for multi-phase incompressible flow. *J. Sci. Comput.*, vol. 15, pp. 323–360.
- Kumar, P.; Gompper, G.; Lipowsky, R.** (2001): Budding dynamics of multicomponent membranes. *Phys. Rev. Lett.*, vol. 86, pp. 3911.
- Kumar, P.; Rao, M.** (1998): Shape instabilities in the dynamics of a two-component fluid membrane. *Phys. Rev. Lett.*, vol. 80, pp. 2489.
- Landau, L.** (1984): *Statistical physics*. Butterworth-Heinemann, Oxford.
- Laradji, M.; Kumar, P.** (2004): Dynamics of domain growth in self-assembled fluid vesicles. *Phys. Rev. Lett.*, vol. 93, pp. 198105.
- Lavrenteva, O.; Tsemakh, D.; Nir, A.** (2005): Locomotion of a viscous drop, induced by the internal secretion of surfactant: Boundary effects. *FDMP: Fluid Dynamics & Materials Processing*, vol. 1, pp. 131.
- LeVeque, R.; Li, Z.** (1994): The immersed interface method for elliptic equations with discontinuous coefficients and singular sources. *SIAM J. Numer. Anal.*, vol. 31, pp. 1019–1044.
- LeVeque, R.; Li, Z.** (1997): Immersed interface methods for stokes flow with elastic boundaries or surface tension. *SIAM. J. Sci. Comput.*, vol. 18, pp. 709.
- Li, Z.; Ito, K.; Lai, M.-C.** (2007): An augmented approach for stokes equations with a discontinuous viscosity and singular forces. *Comp. Fluids*, in press., 2007.

- Lipowsky, R.** (1991): The conformation of membranes. *Nature*, vol. 349, pp. 475.
- Lipowsky, R.; Sackman, E.**(Eds): *Structure and dynamics of membranes— From cells to vesicles, Vols. 1A/B*. Elsevier, Amsterdam.
- Lowengrub, J.; Truskinovsky, L.** (1998): Quasi-incompressible cahn-hilliard fluids and topological transitions. *Proc. R. Soc. London Ser. A*, vol. 454, pp. 2617.
- Macklin, P.; Lowengrub, J.** (2005): Evolving interfaces via gradients of geometry-dependent interior poisson problems: application to tumor growth. *J. Comp. Phys.*, vol. 203, pp. 191.
- Macklin, P.; Lowengrub, J.** (2006): An improved geometry-aware curvature discretization for level-set methods: Application to tumor growth. *J. Comp. Phys.*, vol. 215, pp. 392.
- McMahon, H.; Gallop, J.** (2005): Membrane curvature and mechanisms of dynamic cell remodelling. *Nature*, vol. 438, pp. 590.
- Mukherjee, S.; Maxfield, F.** (2004): Membrane domains. *Ann. Rev. Cell. Dev. Biol.*, vol. 20, pp. 839.
- Nelson, D.; Piran, T.; Weinberg, S.**(Eds): *Statistical mechanics of membranes and surfaces*. World Scientific, Singapore.
- Osher, S.; Fedkiw, R.** (2001): Level set methods: An overview and some recent results. *J. Comp. Phys.*, vol. 169, pp. 463.
- Osher, S.; Sethian, J.** (1988): Fronts propagating with curvature dependent speed: algorithms based on hamilton-jacobi formulations. *J. Comp. Phys.*, vol. 79, pp. 12.
- Pozrikidis, C.** (1992): *Boundary integral and singularity methods for linearized viscous flow*. Cambridge University Press, Cambridge.
- Pozrikidis, C.** (2001): Interfacial dynamics for stokes flow. *J. Comp. Phys.*, vol. 169, pp. 250.
- Ramaswamy, S.; Toner, J.; Prost, J.** (2000): Nonequilibrium fluctuations, traveling waves and instabilities in active membranes. *Phys. Rev. Lett.*, vol. 84, pp. 3494.
- Reigada, R.; Buceta, J.; Lindenberg, K.** (2005): Generation of dynamic structures in nonequilibrium reactive bilayers. *Phys. Rev. E*, vol. 72, pp. 51921.
- Reigada, R.; Buceta, J.; Lindenberg, K.** (2005): Nonequilibrium patterns and shape fluctuations in reactive membranes. *Phys. Rev. E*, vol. 71, pp. 51906.
- Sethian, J.; Smereka, P.** (2003): Level set methods for fluid interfaces. *Ann. Rev. Fluid Mech.*, vol. 35, pp. 341.
- Shi, Q.; Voth, G.** (1993): Multiscale modeling of phase separation in mixed lipid bilayers. *Biophys. J.*, vol. 89, pp. 2385.
- Shu, C.-W.** (1988): Total-variation-diminishing time discretization. *SIAM J. Sci. Stat. Comput.*, vol. 9, pp. 1073.
- Sussman, M.; Smereka, P.; Osher, S.** (1994): A level set approach for computing solutions to incompressible two-phase flow. *J. Comput. Phys.*, vol. 114, pp. 146–159.
- Taniguchi, T.** (1996): Shape deformation and phase separation dynamics of two-component vesicles. *Phys. Rev. Lett.*, vol. 76, pp. 4444.
- Uchida, N.** (2002): Dynamics of orientational ordering in fluid membranes. *Phys. Rev. E*, vol. 66, pp. 04092.
- Veatch, S.; Keller, S.** (2003): Separation of liquid phases in giant vesicles of ternary mixtures of phospholipids and cholesterol. *Biophys. J.*, vol. 85, pp. 3074.
- Xu, J.; Li, Z.; Lowengrub, J.; Zhao, H.** (2006): A level set method for solving interfacial flows with surfactant. *J. Comp. Phys.*, vol. 212, pp. 590–616.
- Xu, J.; Zhao, H.** (2003): An eulerian formulation for solving partial differential equations along a moving interface. *J. Sci. Comp.*, vol. 19, pp. 573–594.

**Zhao, H.; Chan, T.; Merriman, B.; Osher, S.** (1996): A variational level set approach to multiphase motion. *J. Comp. Phys.*, vol. 127, pp. 179–195.

**Zhong-can, O.-Y.; Helfrich, W.** (1989): Bending energy of vesicle membranes: General expressions for the first, second and third variation of the shape energy and applications to spheres and cylinders. *Phys. Rev. A*, vol. 39, pp. 5280.

